ENHANCING THE ATOMIC-LEVEL UNDERSTANDING OF CO_2 MINERAL SEQUESTRATION MECHANISMS VIA ADVANCED COMPUTATIONAL MODELING

Type of Report:	Year 1 Technical Progress
Reporting Period Start Date:	9/20/01
Reporting Period End Date:	9/20/02
Principal Author:	A.V.G. Chizmeshya*
Co-Investigators:	M.J. McKelvy and O.F. Sankey
Date Report Issued:	December 19, 2002
DOE Award Number:	DE-FG26-01NT41295
Submitting Organization:	Arizona State University Center for Solid State Science Tempe, AZ 85287-1704

* Phone: (480) 965-6072; FAX: (480) 965-9004
e-mail: chizmesh@asu.edu

DISCLAIMER

ABSTRACT

Fossil fuels currently provide 85% of the world's energy needs, with the majority coming from coal, due to its low cost, wide availability, and high energy content. The extensive use of coal-fired power assumes that the resulting CO_2 emissions can be vented to the atmosphere. However, exponentially increasing atmospheric CO_2 levels have brought this assumption under critical review. Over the last decade, this discussion has evolved from whether exponentially increasing anthropogenic CO_2 emissions will adversely affect the global environment, to the timing and magnitude of their impact. A variety of sequestration technologies are being explored to mitigate CO_2 emissions. These technologies must be both environmentally benign and economically viable. Mineral carbonation is an attractive candidate technology as it disposes of CO_2 as geologically stable, environmentally benign mineral carbonates, clearly satisfying the first criteria. The primary challenge for mineral carbonation is cost-competitive process development.

CO_2 mineral sequestration – the conversion of stationary-source CO_2 emissions into mineral carbonates (*e.g.*, magnesium and calcium carbonate, $MgCO_3$ and $CaCO_3$) – has recently emerged as one of the most promising sequestration options, providing *permanent* CO_2 disposal, rather than storage. In this approach a magnesium-bearing feedstock mineral (typically serpentine or olivine; available in vast quantities globally) is specially processed and allowed to react with CO_2 under controlled conditions. This produces a mineral carbonate which (i) is environmentally benign, (ii) already exists in nature in quantities far exceeding those that could result from carbonating the world's known fossil fuel reserves, and (iii) is stable on a geological time scale. Minimizing the process cost *via* optimization of the reaction rate and degree of completion is the remaining challenge.

As members of the DOE/NETL managed National Mineral Sequestration Working Group we have already significantly improved our understanding of mineral carbonation. Group members at the Albany Research Center have recently shown that carbonation of olivine and serpentine, which naturally occurs over geological time (i.e., 100,000s of years), can be accelerated to near completion in hours. Further process refinement will require a synergetic science/engineering approach that emphasizes simultaneous investigation of both thermodynamic processes and the detailed microscopic, atomic-level mechanisms that govern carbonation kinetics.

Our previously funded Phase I Innovative Concepts project demonstrated the value of advanced quantum-mechanical modeling as a complementary tool in bridging important gaps in our understanding of the atomic/molecular structure and reaction mechanisms that govern CO_2 mineral sequestration reaction processes for the model Mg-rich lamellar hydroxide feedstock material $Mg(OH)_2$. In the present simulation project, improved techniques and more efficient computational schemes have allowed us to expand and augment these capabilities and explore more complex Mg-rich, lamellar hydroxide-based feedstock materials, including the serpentine-based minerals. These feedstock materials are being actively investigated due to their wide availability, and low-cost CO_2 mineral sequestration potential.

Cutting-edge first principles quantum chemical, computational solid-state and materials simulation methodology studies proposed herein, have been strategically integrated with our new DOE supported (ASU-Argonne National Laboratory) project to investigate the mechanisms that govern mineral feedstock heat-treatment and aqueous/fluid-phase serpentine mineral carbonation *in situ*. This unified, synergetic theoretical and experimental approach will provide a deeper understanding of the key reaction mechanisms than either individual approach can alone. *Ab initio*

techniques will also significantly advance our understanding of atomic-level processes at the solid/solution interface by elucidating the origin of vibrational, electronic, x-ray and electron energy loss spectra observed experimentally.

TABLE OF CONTENTS

1. INTRODUCTION

The main focal point of the modeling effort in YEAR 1 of the present Innovative Concepts II award, DE-FG26-01NT41295, has been to explain and elucidate the microscopic origin of structural modifications in lizardite due to heat induced dehydroxylation. Robust, quantitative structural models of the modified mineral are a necessary prerequisite for the subsequent study of carbonation in these materials (see work plan for year 2-3 of the current award performance period, reproduced from the Original proposal in Appendix 2 of the present document). A preliminary account of the first accomplishment has been published in a conference proceeding. Archival journal articles describing both accomplishments are soon to be submitted for publication. The following Technical Progress Report describes research achievements during the first year of performance.

2. EXECUTIVE SUMMARY

2.1 OBJECTIVES

The objective of this project is to use advanced first-principles simulation techniques in concert with experimental observations to develop a detailed, quantitative, atomic-level understanding of aqueous-solution serpentine carbonation mechanisms. The goal is to develop the necessary atomic-level understanding to facilitate the engineering of improved carbonation feedstock materials and reaction processes for CO_2 sequestration. Scientific productivity will be optimized by closely integrating our studies with those being simultaneously performed at the Albany Research Center, and in a joint ASU-Argonne National Laboratory (ANL) study that focuses on *in situ* investigations of aqueous-solution serpentine carbonation reaction mechanisms. Key focal points of our project will include (i) simulation of the morphological changes associated with serpentine heat-activation to understand its role in enhancing carbonation reactivity, (ii) development of a non-empirical site reactivity model for CO_2 with serpentine, and (iii) detailed investigation of the serpentine surface dissolution mechanisms that govern carbonation kinetics, and (iv) the use of first-principles methods to provide deeper atomic-level insight into the mechanistic experimental observations in the partner ASU/ANL studies (*e.g.*, *in situ* studies of reaction intermediate formation).

2.2 ACCOMPLISHMENTS TO DATE

Personnel: Shortly after the establishment of the financial accounting we circulated advertisements for a graduate research assistant (GRA) and for an undergraduate research assistant (URA). In early December we interviewed a number of candidates and subsequently hired two very promising students. The graduate researcher is Ms. Deirdre Gormley, a Science and Engineering of Materials program doctoral candidate. She was selected because of her strong quantum mechanics and previous modeling and computation background. Her start date is January 1, 2002. The URA position has been filled by Mr. Michael Kocher, a senior undergraduate completing a joint Physics-Chemistry bachelor's degree program. Michael has an excellent background in computing and programming and will assist in retrieval, organization and analysis of numerical data generated by our simulation programs.

Equipment and Software: The DMol^3 computer program (Accelrys Inc.) was purchased on schedule, and installed on one of our Facility SGI Workstation/Servers in mid-October. Benchmark calculations on simple oxides (MgO, $Mg(OH)_2$) and gas phase systems (H_2O, CO_2) were performed within the first month of the award period by the principal author. The dedicated dual-processor computational workstation intended for production runs, which was ordered in October, did not arrive until 11/10/01. In the interim, *ab initio* modeling was carried out on a comparable set of machines owned by co-PI Prof. O.F. Sankey, as well as on other shared ASU resources (listed in the award proposal). The dedicated project workstation, together with the software required to execute the proposed research, was fully tested and operational on 11/19/01.

Technical Highllights:

- State-of-the-art quantum mechanical simulation methods were used to predict the existence of a novel, metastable, meta-serpentine material in which order and disorder coexist. This was used to explain the unusual progression of x-ray diffraction patterns observed in association with the heat treatment of serpentine feed stock minerals. Studies were undertaken to elucidate the origin of dehydroxylation mechanisms via simulation of early stage decomposition (%OH loss in the 0-15% range).

- First principles simulation of the subtle structural changes associated with initial dehydroxylation led a new method for analyzing x-ray data − Differential Diffraction Analysis − in which small, systematic XRD spectral changes are simulated and compared with experiment directly. By separating the effect of chemical modification from bonding/coordination changes the method provides new insight into structure modification.

- Modeling and Simulation research results presented at the 27th International Coal Utilization and Fuel Systems conference in Tampa, Florida at the beginning of March 2002.

- Equation of state properties: Completed benchmark simulation of solid phases of 1T-Lizardite ($Mg_3Si_2O_5(OH)_4$), MgO, $Mg(OH)_2$, SiO_2 a-quartz, $MgCO_3$, and gas phase CO_2, and H_2O. The purpose is to generate data needed for end-member/product-phase vertical reaction enthalpies. Structural models based on these simulations are necessary as input for subsequent modeling studies.

- Request for supercomputer resources at the National Energy Research Supercomputer Center (NERSC), and at the Pittsburgh Supercomputing Center (PSC). An initial startup grant was awarded by the PSC on April 24, 2002 providing the theory group at ASU with 50 units on a CRAY platform. This allocation will be used to initiate the serpentine-mineral-surface/aqueous-interface study aimed at elucidating the dissolution and surface chemistry processes under target experimental solution conditions. We anticipate additional allocation awards in connection with the planned aqueous mineral reaction investigations in YEAR 2.

- Modeling of x-ray spectra collected under target conditions (2300 psi/180^{o}C) at the Advanced Photon Source (Argonne National Laboratory) in the 640^{o}C heat treated sample. Focus on MIE-like particle scattering features at low-angle in the XRD spectrum.

- First principles simulations were used to predict the frequencies of infrared absorption bands in the baseline feedstock mineral. Our work provides the first unambiguous assignment of hydroxyl band features in lizardite: silica-cage vibrations are higher in frequency than their brucite-layer counterparts. Simulations will be used to correlate shifts in frequency with changes in local structure during feedstock pre-treatment and carbonation.

- Supercomputer-based quantum molecular dynamics studies of the temperature dependence of the dehydroxylation process have been initiated. This involves the calculation of water formation rate and diffusivities of mineral (and product) components (Mg, Si, OH, H_2O and protons).

2.3 SIGNIFICANCE TO FOSSIL ENERGY PROGRAMS

Fossil fuels, especially coal, can support the energy demands of the world for centuries to come, if the environmental problems associated with CO_2 emissions can be overcome[1-2]. Mineralization of stationary-source CO_2 emissions as carbonates can provide safe capture and long-term sequestration[3-4]. Carbonation of Mg-rich lamellar-hydroxide-based minerals (*e.g.*, the model $Mg(OH)_2$ system and serpentine based minerals) is a leading process candidate, which generates the stable, naturally-occurring mineral magnesite ($MgCO_3$). Optimizing the carbonation reaction rate and its degree of completion are key to process cost and viability. This project focuses primarily (but not exclusively) on the carbonation reaction process mechanisms in serpentine minerals at the atomic level. Carbonation and treatment processes in the olivine class of feedstock minerals will also be briefly studied in support of the research being carried out by the National Mineral Sequestration Working Group managed by NETL. In both cases, the objective is to provide the mechanistic understanding to accelerate the engineering development of improved carbonation materials and processes for carbon dioxide disposal.

3. KEY RESULTS AND DISCUSSION

3.1 Feedstock Pre-processing and the Effects of Heat Treatment: Background

Mg-rich minerals, such as brucite ($Mg(OH)_2$), olivine (*e.g.*, forsterite: Mg_2SiO_4), and serpentine ($Mg_3Si_2O_5(OH)_4$), represent a related class of materials that are particularly well suited for this application. Among these, both serpentine and olivine deposits are common throughout the world. Serpentine-based CO_2 mineral sequestration is particularly appealing, as global serpentine deposits can be mined at low cost and in vast. Enhancing the carbonation reaction rate is the key to lowering process cost, as longer reaction times dramatically increase cost.[5-7] This is the primary focus of the CO_2 Mineral Sequestration Working Group managed by the U.S. Department of Energy, consisting of members from the Albany Research Center, Arizona State University, Los Alamos National Laboratory, the National Energy Technology Laboratory, and Science Applications International Corporation. The low-cost potential offered by serpentine CO_2 mineral sequestration has been recognized by the Zero Emission Coal Alliance (ZECA); an organization of researchers from Los Alamos National Laboratory and U.S. and Canadian coal suppliers and

utilities. Again, the key is increasing the serpentine carbonation reaction rate enough to allow economically viable CO_2 sequestration process development.

Recently our working group colleagues at the Albany Research Center have made exciting breakthroughs by showing that aqueous-solution CO_2 mineral carbonation reactions can accelerate Mg-rich mineral carbonation from the naturally occurring geological time scale (100,000's years) to less than an hour under moderate temperature and CO_2 pressure conditions[6]. The key reactions for serpentine and olivine/forsterite, respectively, are as follows:

$$Mg_3Si_2O_5(OH)_4 + 3\ CO_2 \rightarrow MgCO_3 + 2\ SiO_2 + 2\ H_2O + 64\ kJ/mol \qquad (1)$$

$$Mg_2SiO_4 + 2\ CO_2 \rightarrow MgCO_3 + SiO_2 + 95\ kJ/mol \qquad (2)$$

The carbonation of unpretreated serpentine is found to be significantly slower than that observed for olivine.[8] However, serpentine is much more plentiful in readily mineable deposits worldwide, making it the CO_2 sequestration feedstock material of choice *if its carbonation reactivity can be further enhanced*. When serpentine is heat pretreated for several hours at over 600°C, its carbonation rate has been found to increase dramatically. 70-85% carbonate conversion has been

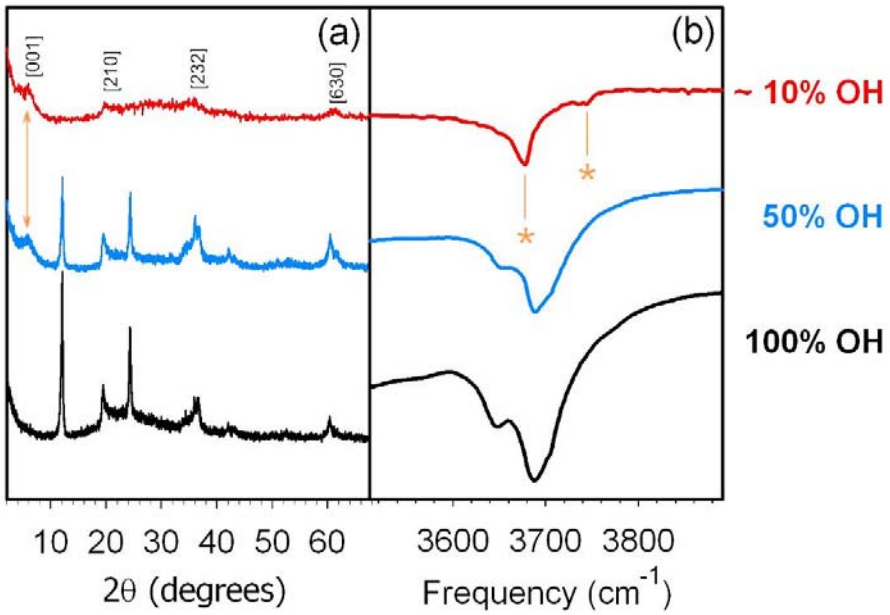

Figure 1: XPD patterns and IR spectra for heat treated Globe lizardite (see preceding companion article for additional details). Black traces: Reference lizardite material under ambient conditions; blue traces: meta-serpentine (heated to 600°C) containing 50% residual hydroxyl, red traces: meta-serpentine (heated to 680°C) containing ~10% residual hydroxyl. Orange arrow in (a) indicates a new low-angle feature in the XPD pattern; asterisks in (b) indicate new vibrational features in the IR data (see preceding companion article for data sequence).

achieved in ~ 1hr (~150°C and 115-185 atm CO_2), exceeding the 1hr conversion rate observed for olivine by an order of magnitude. Unfortunately, heat pretreatment is energy intensive and cost prohibitive. As discussed in the preceding article, an atomic-level understanding of the mechanism(s) by which heat pretreatment enhances serpentine carbonation reactivity is crucial to being able to engineer more cost-effective pretreatment processes. However, many of the important

factors that govern serpentine heat-activation *via* dehydroxylation are only observable at the atomic level.

The infrared (IR) and x-ray powder diffraction (XPD) data for Globe A lizardite, collected as a function of % hydroxyl content, point to a complex relationship between the structural evolution of the system, its extent of dehydroxylation, and ultimately its reactivity with CO_2. We have reproduced a portion of the IR and XPD data sequence in Figure 2, above. The corresponding XPD spectra evolve from that of the baseline lizardite (black trace) to an intermediate meta-serpentine material (red trace), with what appears to be a doubled c lattice parameter (a stage-2 lamellar meta-serpentine intermediate material), as evidenced by the new low-angle reflection near $2\theta \sim 6^{o}$. The corresponding vibrational spectra (shown in the right panel of the figure) reveal a concomitant shift in the hydroxyl band frequencies accompanying the formation of the meta-serpentine. Further heating leads to amorphization, and upon complete dehydroxylation, by the condensation into an assemblage of Mg_2SiO_4 (forsterite) and $MgSiO_3$ (enstatite). Clearly the detailed interpretation of the IR and XPD behavior with respect to variation in hydroxyl content requires a structural model. This is the focus of our recent modeling activity. The goal is to relate the observed spectroscopic observations to an atom-level decription of the heat-activated lizardite.

Our general approach to modeling these systems is to first generate model structures which correspond *precisely* the stoichiometry of the observed meta-serpentines. Relaxation of the volume and atomic positions using accurate quantum mechanical forces and total energy is then expected to provide plausible meta-serpentine representations which can then be subsequently used in the simulation of vibrational, electronic and elastic behavior. We use two schemes to generate hypothetical structures: (i) beginning with an appropriate supercell of lizardite we remove a stoichiometric amount of water to produce meta-serpentine, and (ii) we start with an assemblage of $MgSiO_3$ and Mg_2SiO_4 and add water to achieve the target stoichiometry. In the present work we adopt the first approach, and focus on the interpretation of XPD and IR spectra discussed in the preceding article on heat-activated lizardite.

3.1.1 Static Ground State Crystalline Simulations

As a preliminary step to simulating lizardite, and "meta-lizardite" we computed the ground state properties and compression equation of state of a number of related oxide materials: MgO, $Mg(OH)_2$, $MgSiO_3$. In addition to providing a necessary check on the numerical procedure, valuable structural, electronic and elastic information is also generated in the process.

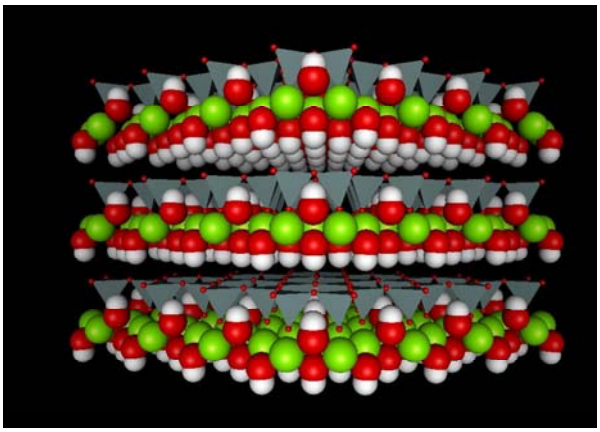

Figure 2: Model representation of the 1T-Lizardite polymorph of serpentine mineral feedstock showing approximately 48 unit cells (16 per layer).

Our calculations were performed using the first-principles total-energy VASP code[9], which employs a plane-wave basis and ultrasoft pseudopotentials within density functional theory. The exchange-correlation effects are treated with the local density ap-proximation[10] (LDA) using the Ceperley-Alder functional[11], or with the generalized gradient approximation[10]

(GGA). The compression equation of state was computed by optimizing the crystalline structures (cell parameters as well as internal parameters) for a series of volumes spanning a range of about –15% to +40% about the experimentally observed ambient pressure volume. We used an energy cutoff of 600 eV for the plane wave basis to ensure good convergence of the state properties. Several dozen special *k*-points were used for the dense systems, whereas Γ-point sampling was sufficient for systems like lizardite. However, as we shall show below, a reliable prediction of the internal crystalline structure of lizardite requires a denser (more computationally expensive) *k*-point integration grid.

A conjugate-gradient technique was used to drive the fixed volume structures to a minimum force configuration.

System	E_0 (eV/atom)	V_0 (Å^3/atom)	K (GPa)	K′
MgO (Periclase)	-5.827	9.10 (**9.35**)	172 (**160**)	4.0 (**4.0**)
$Mg(OH)_2$ (Brucite)	-4.879	7.33 (**8.02**)	65 (**45**)	5.2 (**5.7**)
$MgSiO_3$ (Enstatite)	-6.803	10.45 (**10.48**)	125 (**121**)	3.1 (**3.8**)
$Mg_3Si_2O_5(OH)_4$ (1T-Lizardite)	-5.844	9.38 (**9.91**)	78 (*)	7.3 (*)

Table 1. Experimental and theoretical parameters of the Birch-Murnaghan equations of state for MgO ($Fm\bar{3}m$ symmetry), $Mg(OH)_2$ ($P\bar{3}m1$), $MgSiO_3$ (*Pbcn*) and $Mg_3Si_2O_5(OH)_4$ (*P31m*). The tabulated values for the binding energy (E_0), equilibrium volume (V_0), zero-pressure bulk modulus (K) and P=0 bulk modulus pressure derivative (K′) were obtained by fitting our energy vs. volume data to a third-order Birch-Murnaghan equation of state. Experimental data shown in bold face from Ref.[12]. An asterisk indicates that the value has not yet been measured and/or reported.

The LDA results are summarized in Table 1 and indicate that the simulations generally give a very good account of experimental trends. The binding energies represent the difference between the crystalline energy and neutral atoms, divided by the total number of atoms per unit cell. The predicted internal unit cell parameters and lattice constants for brucite, enstatite and lizardite (not shown) are found to agree with experiment to better than 1%, except for in the case of brucite and lizardite, where the interlayer binding is overestimated by the LDA. This results in the *c*-parameter being slightly underestimated compared with experiment. The tendency of the LDA to underestimate bond lengths (and therefore volume) is well known. As can be seen from the table, this effect leads to a concomitant increase in the bulk moduli relative to experiment.

In carrying out the fixed volume internal structure optimizations described above no shape constraint was imposed upon the computational cells. The associated stress tensor exhibited negligible anisotropy indicating no departure from hexagonal symmetry. After each complete equation of state determination we also performed a highly accurate full stress relaxation starting with a volume and lattice configuration close to equilibrium, and obtained the same equilibrium volume as determined from a energy-volume fit. This procedure also yields the detailed internal atomic structure of the mineral. A plane wave basis cutoff of 1000eV (using projected-augmented

wave (PAW) type ultrasoft pseudopotentials[9]) was used to ensure a high level of convergence of the energy and atomic forces within the system. The *k*-space integrations were carried out using 1x1x1 and 2x2x1 Monkhorst-Pack grids and Gamma point centering. The results for the 1x1x1 and 2x2x1 calculations are presented in Tables 2 and 3, respectively, where they are compared with the experimental structural data of Guggenheim and Zhan[13].

Atom	**LDA**			***GGA***			***Experiment***		
a (Å)	5.1524			5.2750			**5.3267**		
c (Å)	7.1101			7.4037			**7.2881**		
	x	y	z	x	y	z	**x**	**y**	**z**
Mg	0.331	0	0.454	0.331	0	0.451	**0.332**	**0**	**0.455**
Si	1/3	2/3	0.064	1/3	2/3	0.070	**1/3**	**2/3**	**0.074**
O1	1/3	2/3	0.286	1/3	2/3	0.287	**1/3**	**2/3**	**0.291**
O2	0.602	0	-0.014	0.592	0	-0.005	**0.507**	**0**	**-0.008**
O3	0.664	0	0.592	0.664	0	0.586	**0.664**	**0**	**0.588**
O4	0	0	0.296	0	0	0.303	**0**	**0**	**0.304**
H1	0.660	0	0.729	0.658	0	0.717	**0.583**	**0**	**0.732**
H2	0	0	0.159	0	0	0.172	**0**	**0**	**0.197**

Table 2: LDA and GGA calculations of the internal structure (in fractional coordinates) and unit cell parameters (in Angstroms) of 1T-Lizardite. Single *k*-point (*k*=0) sampling was used in the reciprocal space integrations.

From an examination of these tables it is clear that the GGA slightly overestimates the lattice parameters while the LDA yields a slight underestimate relative to experimental observation. However, the overall predictive ability of density functional theory is remarkable. The internal positions of all the heavy atoms are extremely well reproduced, especially using the 2x2x1

Atom	**LDA**			***GGA***			***Experiment***		
a (Å)	5.2653			5.3633			**5.3267**		
c (Å)	7.0904			7.4167			**7.2881**		
	x	y	z	x	y	z	**x**	**y**	**z**
Mg	0.331	0	0.456	0.331	0	0.453	**0.332**	**0**	**0.455**
Si	1/3	2/3	0.067	1/3	2/3	0.074	**1/3**	**2/3**	**0.074**
O1	1/3	2/3	0.290	1/3	2/3	0.291	**1/3**	**2/3**	**0.291**
O2	0.531	0	-0.020	0.514	0	-0.008	**0.507**	**0**	**-0.008**
O3	0.664	0	0.591	0.664	0	0.585	**0.664**	**0**	**0.588**
O4	0	0	0.298	0	0	0.303	**0**	**0**	**0.304**
H1	0.660	0	0.729	0.650	0	0.715	**0.583**	**0**	**0.732**
H2	0	0	0.159	0	0	0.173	**0**	**0**	**0.197**

Table 3: As for Table 2 but with reciprocal space integrations evaluated using a 2x2x1 Monkhorst-Pack grid.

integration grid and GGA (Table 3). The only minor discrepancy is found in the prediction of the hydroxyl bond lengths which are estimated to be 0.02-0.06 Å too long. It is also noteworthy that the GGA also overestimates the c-axis cell parameter by about 0.13 Å (for the 2x2x1 GGA case). This is not surprising since it is well known that non-local correlation effects, *e.g.*, van der Waals bonding, are not included at this level of theory. In spite of this the agreement is excellent and more than sufficient in terms of predictive accuracy for all of our subsequent modeling studies.

3.1.1(a) Initial stages of Dehydroxylation

Combined thermogravimetric and x-ray diffraction analysis indicates that the dehydroxylation induced by heat-treatment produces a gradual change in the structure and composition of the lizardite. An understanding of the structural origin of carbonation reactivity enhancement in heat-treated lizardite seems to be related to the microscopic structure, *e.g.*, the access to reactive sites such as under-coordinates oxygen ions, etc. In order to systematically explore the effect of heat-treatment and water loss on the solid-state structure of the mineral we undertook the study of 12.5% dehydroxylated materials. This corresponding to one out of every eight hydroxyls being removed from the system. To model this system we adopted a large periodic supercell representation of the mineral with sufficient extent to ensure that individual defects (missing protons and hydroxyls) do not significantly interact with their periodic images in neighboring cells. *Ab initio* simulation methods (*e.g.*, the VASP code) were used to elucidate the dehydroxylation reaction, including water formation, in the early stages of heat-treatment in serpentine. Very precise comparisons of the structural trends in going from the baseline (untreated) material to a slightly dehydroxylated sample can be obtained in this way. The main focus is on the initial modifications of the "lizardite" system due to the water loss, and in particular on the implications for the XRD spectra. Figure 3 illustrates schematically two specific water loss/de-hydroxylation scenarios labeled as heteroplanar, involving neigh-boring planes separated by the inter-lamellar gallery, and homoplanar, in which water is formed from neighboring hydroxyls and protons from within the same "brucite"-like layer.

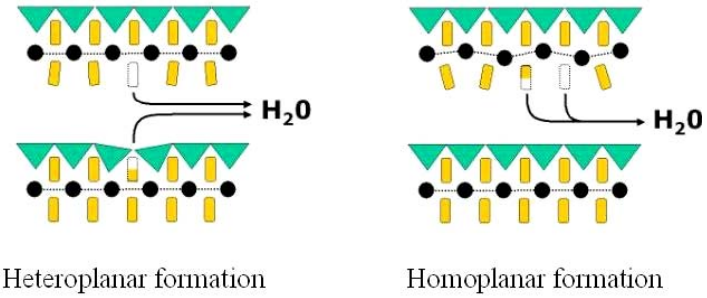

Figure 3: Simplified conceptual models of the dehydroxylation process in lizardite. Green triangles represent the silica sheet tetrahedral; black filled circles: Mg; yellow rectangles: hydroxyls and hollow and semi-hollow rectangles: hydroxyl and proton vacancies, respectively.

For stoichiometric 1T-lizardite we have identified four candidate dehydroxylation paths involving various combinations of "brucite-like" and "cage" hydroxyls and protons. Typical configurations are illustrated schematically in Figure 4. The configurations are labeled by two consecutive letters: "B" and/or "C" denoting "brucite"-layer and "cage"-layer protons and/or hydroxyl species. Thus, the configuration CB (not shown in the figure) designates water formation from a cage hydroxyl and a brucite-layer proton while "BB" represents the homoplanar mechanism shown in the right panel of Figure 3. These choices for the configurations assume that the most

energetically accessible water formation routes involve nearest neighbor proton-hydroxyl combinations. However, both homo-planar and hetero-planar situations are considered.

All of the defective (dehydroxylated) unit cells (BB,BC,CB and CC) were derived from an structurally optimized stoichiometric lizardite cell of composition $Mg_3Si_2O_5(OH)_4$ (s) by simple removal of the desired hydroxyl/proton pair according to the procedure described above. We calculated the vertical reaction energy, ΔE, for endothermic formation of the 12.5 % dehydroxylated material according to:

$$4\ Mg_3Si_2O_5(OH)_4(s) \rightarrow Mg_{12}Si_8O_{21}(OH)_{14}(s) + H_2O(g) + \Delta E \qquad (3)$$

The static ground state energy of a gas-phase water was estimated by placing a single molecule into a large cubic supercell of edge length ~ 8 Å. Convergence was obtained by varying the plane-wave cutoff and the cell size until changes of less than ~0.01eV in the total energy were observed. After 41 steps, the defective structure reached its ground state. All calculations were carried out on a Pentium IV dual processor workstation using the highly efficient *ab initio* VASP code. For each case considered the equilibrium structure (ground state) of the defective lizardite was obtained by minimizing the quantum mechanical forces on all of the atoms/ions. The unit cell parameters (cell length edges and inter-axial angles) were also determined by simultaneously minimizing the external stress tensor. Full details of our calculations and results are being written up as an archival journal article (see Appendix 1).

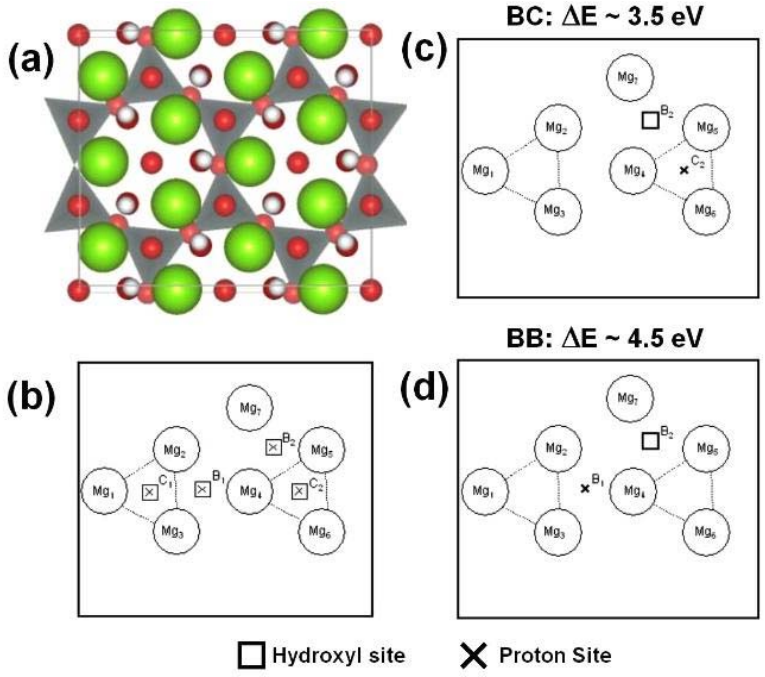

Figure 4: (a) Atomic positions of the relaxed lizardite reference structure prior to dehydroxylation reaction , (b) schematic legend indicating the location of: "brucite"-layer (B) and silica cage (C) defect sites. (c) the least metastable BC configuration in which a hydroxyl group is removed from a B site and a proton vacates a C site; (d) most metastable (least favorable) BB configuration, water formation from within a brucite layer.

To summarize, our simulations predict a systematic dilation of Mg-Mg bonds in the vicinity of hydroxyl vacancies, leading to a decoherence in x-ray scattering intensity for reflections originating from these planes. Furthermore, a systematic *decrease* is predicted for the c-axis in the defective structures. Perhaps surprisingly, the least *metastable* structure is BC involving the formation of water from a "brucite"-layer hydroxyl and an abstracted proton from a silica-cage site. The defect formation energies for BB, CB and CC are also positive and range in value from 3.5 to 4.5 eV per H_2O desorbed (*e.g.*, 338 to 435 kJ/mol). It is significant that the spread in defect formation energies is small. This suggests that all of the candidate mechanisms considered may be thermodynamically important in the dehydroxylating mineral. Accordingly, the actual XRD pattern of the meta-lizardite may best be modeled by averaging of the individual XRD patterns for BB, BC, CB and CC configurations according to their Boltzmann weighted energies relative to the lowest energy configuration, BC, at finite temperature.

Differential XRD Analysis: A powerful bridge between Experiment and Theory

The point of contact with experiment is made by comparing the x-ray patterns measured in the laboratory with the synthetic patterns obtained from our predicted structural models. The model x-ray scattering intensities (synthetic powder patterns) were calculated using the *Cerius*[2] package (Accelrys Inc.) using a preferred orientation along (001), which is consistent with the experimental data, and a March-Dollase function parameter of R_0=0.7. The numerical difference between two integrated x-ray diffraction spectra (2θ plots) is exploited in the structural refinement procedure used to derive crystal structures from x-ray data, where it represents the objective function to be minimized. Typically, a synthetic pattern based on an assumed structure is subtracted from the experimental trace and a weighted average of the difference is numerically minimized with respect to the structural parameters in the model to obtain a "best fit" structure. In our case, we seek to interpret the origin of the features in the differential spectrum between two similar materials. The latter pair could be the reference lizardite and a slightly dehydroxylated meta-lizardite, or two neighboring meta-serpentines with similar composition. For small changes in stoichiometry the diffraction patterns of the reference and altered materials are nearly identical, hampering interpretation. However, when the differential spectrum (numerical difference between the two spectra) is examined characteristic features are evident. These are illustrated in left panel of Figure 5, where the effects of structural and chemical change are shown. For examples, a substitutional impurity (Mg ↔Fe) may induce a slight structural change (no shift in peak position) but a significant reduction/increase in peak intensity (top two cases). Alternatively, a systematic trend in the local environment of a given scatterer can lead to a shift in peak position with negligible effect in the intensity. The most general case involves simultaneous combinations of all of these effects.

In the right panel of Figure 5 we illustrate the usefulness of this direct approach by comparing the measured differential patterns for two heat treated samples with the predictions obtained above for the 12.5% meta-lizardite. The most intense reflections in the lizardite system are related to the characteristic length scales of the unit cell. In Table 4 we list the optimized cell parameters for the reference lizardite (designated 100% OH) and the BC 12.5% dehydroxylated model (designated 87.5% OH). The magnitude of the changes in the cell parameters is quite small (~ 0.2%), but the structural coherence of the internal structure is preserved in the defective meta-lizardite. These and related details will be discussed in an upcoming paper (see Appendix 1). These converged (zero-force) structures were used to generate synthetic XRD patterns, and these were

numerically subtracted to yield the black trace in the right panel of Figure 5. The corresponding differential spectrum for the 550°C Philips sample is shown as the green curve while that corresponding to Globe A 580°C/20°C samples is shown in orange. While the experimental traces share some common features it is clear from a comparison with the theoretical trace that the Philips sample is closer to the ideal 1T-lizardite, and its dehydroylate than the Globe A sample.

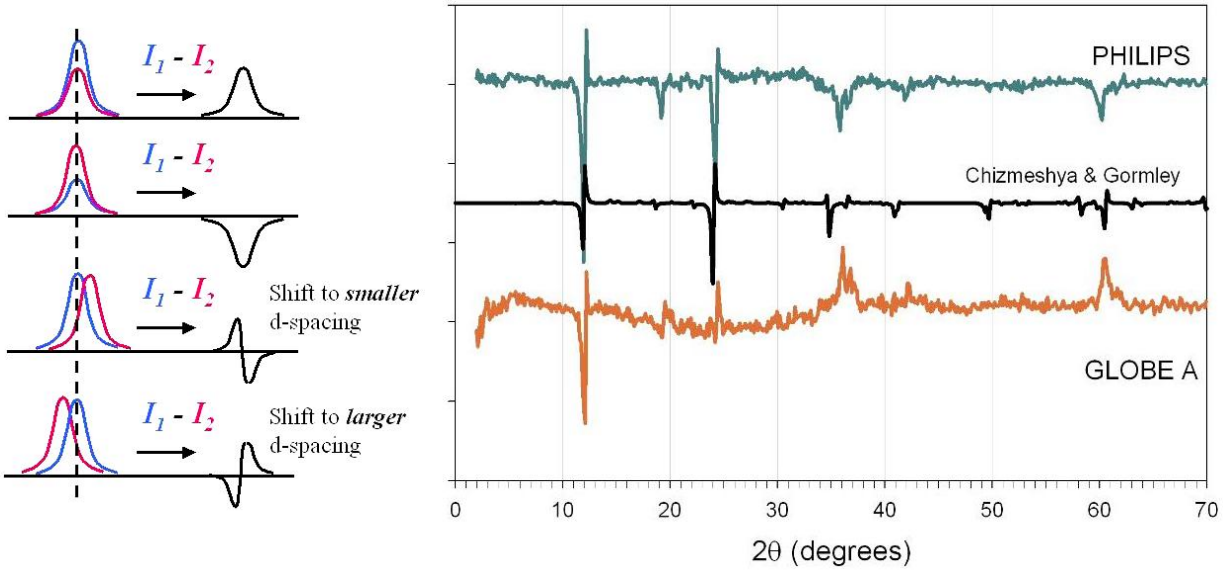

Figure 5: Left panels: Concept schematic illustrating the origin of differential signatures (black curves). Blue curves represent a spectral feature in the reference structure while the red curves denote the corresponding feature in the chemically or structurally altered structure. Right panel: Representative results and comparisons for Philips and Globe A lizardite. The green curve is the differential XRD pattern corresponding to the 550°C Philips sample relative to 20°C spectrum; orange curve: corresponding difference spectrum for Globe A 580°C/20°C samples. Black curve: Theoretical results obtained from first principles simulation.

	$a=2a_L$	$b=\sqrt{3}a_L/2$	$c=c_L$
100% OH	10.780	9.359	7.253
87.5% OH	10.787	9.378	7.238
	0.0 %	**+0.2%**	**-0.2%**

Table 4: Change in cell lattice constants of the 12.5% dehydroxylated lizardite model. Here a_L and c_L refer to the 1T lizardite unit cell parameters (in Angstroms).

3.1.1(b) Structural model for 50% weight loss Meta-Lizardite

Since the initial and strongest appearance of the low-angle meta-serpentine intermediate occurs at 50% dehydroxylation (blue IR and XPD traces in Figure 1), we have initiated our studies based on this as a target composition. Figure 6 illustrates the example of 50% dehydroxylated $Mg_3Si_2O_5(OH)_4$ (lizardite) obtained via scheme (i) described on p.10, Section 3.1. Several dozen

model structures were contructed from a 144-atom (Z=8) supercell of 1T-lizardite by removal of H_2O corresponding to 50% dehydroxylation. These corresponding supercells have stoichiometry $8{\cdot}Mg_3Si_2O_5(OH)_4$ - $8{\cdot}H_2O$ and contain 120 atoms. By experimenting with different strategies for removing the requisite number of OH and H's from the reference cell, we ascertained that the low angle feature near $2\theta \sim 6^o$ can only be reproduced when H_2O is preferentially removed from alternating layers with a ratio of 4:1 or greater. A unit cell corresponding to a 13:3 model is shown in Figure 6(b). It also follows that stage-2 behavior (every other lizardite lamella having different oxide/hydroxide compositions) is optimally found for half of the full hydroxide concentration, in analogy with lamellar de-intercalation reaction mechanisms. Note that the meta-serpentine structures represented in Figure 6 are empirical at this stage, namely, they are based on experimental lattice parameters and internal coordinates. Thus, the simulated XPD patterns do not account for ionic relaxation. Nevertheless, these simple structural models demonstrate that uniform dehydroxylation cannot account for the appearance of the low angle features observed, but non-uniform dehydroxylation can.

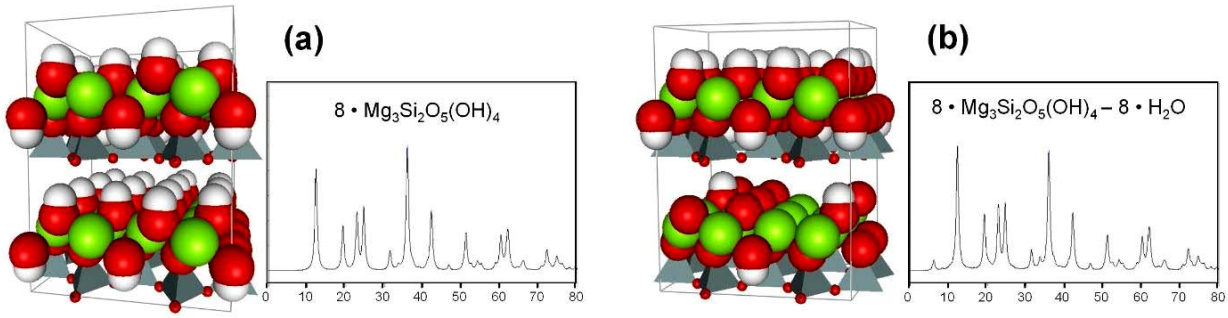

Figure 6: (a) Synthetic XPD pattern for reference material (1T-Lizardite), (b) Meta-serpentine (50% dehydroxylated) obtained by randomly removing OH and H from the reference lizardite in (a) using a target ratio of ~ 1:4 between alternate layers (Legend: H=white, Mg=green, O=red, SiO_4=grey). Horizontal axes: 2θ (degrees).

Using the 50% dehydroxylated meta-serpentine model structure shown in Figure 6(b) above as a starting point we subsequently carried out full structural relaxation calculation for a 120-atom supercell. A high-quality plane-wave basis set with a cutoff of 600 eV was used together with an

System	Cell Parameters (lengths in Å, angles in degrees)	Energy/atom (eV)	Volume/atom (Å^3/atom)	Energy/Formula (eV)
$8{\cdot}Mg_3Si_2O_5(OH)_4$	a = 10.484 $\alpha = 90^o$ b = 9.106 $\beta = 90^o$ c = 14.124 $\gamma = 90^o$	-5.838	9.364	-105.084
$8{\cdot}Mg_3Si_2O_6(OH)_2$	a = 10.486 $\alpha = 90^o$ b = 9.137 $\beta = 91.45^o$ c = 13.987 $\gamma = 90^o$	-5.982	11.165	-89.73

Table 5: Structural relaxation results for the 1T-lizardite supercell and for the 50% dehydroxylated serpentine (meta-serpentine) model.

increased tolerance criterion for the calculation of unit cell stress. Identical computational parameters were also used to optimize a 144-atom supercell of stoichiometric lizardite, so that an accurate energy difference for the dehydroxylation reaction could be determined. Simultaneous optimization of the cell shape and volume as well as the internal positions of the atoms required a very accurate calculation of forces and stresses within the unit cell, and demanded several weeks of continuous computation on a modern dual-processor workstation. Symmetry constraints were not imposed upon the atomic positions within the cell. The results are summarized in Table 5, which lists the relaxed cell parameters, as well as the binding energies. The lizardite results listed here can be directly compared with those listed in Table 1. Small differences arise because slightly less stringent computational conditions were employed for the larger cells. The removal of water to form meta-serpentine, $Mg_3Si_2O_6(OH)_2$, induces a slight monoclinic distortion in the crystalline structure and an increase in the volume per atom. This result suggests that staged dehydroxylation is not correlated with a dramatic volume collapse. From the parameters listed above the unit cell volume decrease amounts to about 1%, but because water was removed the density also is found to decrease from ~ 2.73 g/cc in the simulated lizardite to ~ 2.57 g/cc in the simulated meta-serpentine. Using the energies given in Tables 1 and 5 it is possible to compute the binding energy difference associated with dehydration, *e.g.*,

$$Mg(OH)_2 \rightarrow MgO + H_2O + \Delta U_d. \quad (4)$$

$$Mg_3Si_2O_5(OH)_4 \rightarrow Mg_3Si_2O_6(OH)_2 + H_2O + \Delta U_d. \quad (5)$$

The binding energy of H_2O is computed to be –11.93 eV[14]. This yields a formation enthalpy of 18.7 kcal/mol for reaction (3) which compares well with the observed value of 19.4 kcal/mol[15], while for reaction (4) we obtain a substantially larger value of 79.0 kcal/mol. This large value may be associated with the larger binding energy of the silica sheet hydroxyls compared with their "brucite"-like analogs.

The implications of these calculations for the XPD are illustrated in Figure 7, which shows that the low angle feature is preserved even after relaxation and that the primary reflection near $2\theta \sim 12^o$ (now indexed as 002) is slightly shifted but not significantly attenuated. The slight disordering of the basal plane symmetry in every alternate layer apparently leads to blunting of the reflections in the range $2\theta \sim 40\text{-}80^o$, which is also consistent with the observed XPD pattern. The simulations indicate that dehydroxylation induces comparatively small distortion in the tetrahedral silica layer in spite of the rather significant disordering of the Mg and O sublattices. Preliminary analysis of the bonding within the dehydroxylated layer indicates the presence of several low-coordination oxygen sites which have been experimentally identified as preferred CO_2 adsorption sites in oxide surfaces[16]. Our simulations indicate that the residual hydroxyls within the heavily dehydroxylated bottom layer (figure 4(a)) retain their functionality as pillars and serve to maintain the ~ 7 Å spacing between silica sheets. The stage-2 behavior alluded to above is very common in graphite and transition-metal dichalcogenide deintercalation processes. This suggests that a somewhat similar process may be occurring in the early stages of meta-serpentine formation. The rumpling of the Mg and O sublattice that accompanies stage-2 compound formation is also particularly intriguing, as this may well be related to the enhanced Mg solubility and carbonation reactivity observed for meta serpentine.

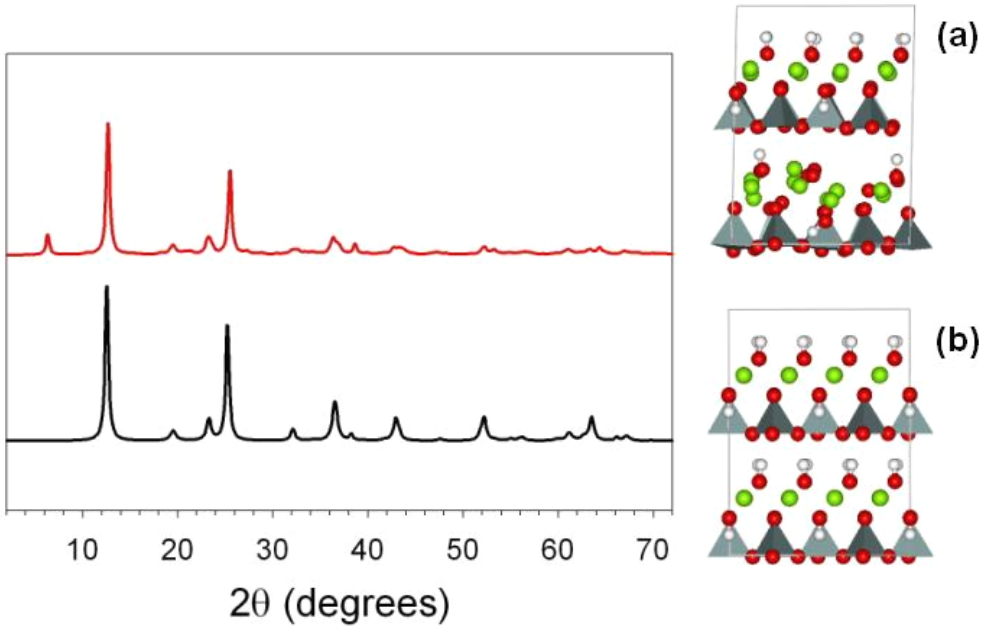

Figure 7: Effects of structural relaxation on the XPD pattern. (a) 50% residual hydroxyl meta-serpentine, (b) initial lizardite structure. Left panel: simulated XPD; black trace: initial lizardite structure, red trace: relaxed meta-lizardite structure. (Legend: H=white, Mg=green, O=red, SiO_4=grey)

The above results are based on a statistical description of plausible defective crystalline configurations for 50% water removal were presented at the 2002 Clearwater conference. Our detailed modeling of the 50% dehydroxlyated material has nicely explained the origin of a number of observed spectroscopic features. However, the precise thermal dehydroxylation mechanism, *e.g.*, diffusion path of OH and H_2O within the decomposing material is has still not been identified. However, this information may be obtained from a full first principles quantum molecular dynamics simulation at finite temperature and pressure. Our work in this area has already been initiated (October of 2002) and preliminary results will be discussed at the 2003 Clearwater conference. A complete detailed summary will be provided in next years Technical Progress Report.

3.1.1(c) Carbonation in 50% weight loss Meta-Lizardite

The natural question arising from the results of the previous section is: Why does the 50% meta-lizardite carbonate more readily? A partial answer is suggested by the modeling study just discussed: The removal of half significant water from the mineral does not necessarily lead to imminent collapse of the structure. Instead, a staging type of behavior is adopted as a low energy state. The open "pillared" configuration of this meta-lizardite may promote rapid diffusion of water and CO_2 under the supercritical conditions observed experimentally. To obtain a preliminary picture of the interaction of CO_2 with meta-lizardite we have carried out a quantum molecular dynamics study using a previously converged 50% model (see 3.1.1(b) above), in which the lattice parameters are a=10.5311 Å, b=9.1732 Å and c=14.0226 Å. The latter values are slightly larger than those reported in Table 5, above, due to thermal expansion. A somewhat large time step of 1.0 fs was used to integrate the equations of motion under constant temperature rescaling conditions and T=450K (*e.g.*, ~177^{o}C). The meta-serpentine lattice was initially prepared by running the

dynamics for about 2.0 ps. The instantaneous velocities were stored and used to initiate a new simulation in which the CO_2 molecule was introduced into the void-like gallery between heavily/lightly dehydroxylated layers in the meta-lizardite. Using the same computational conditions the dynamics was then re-initiated. Minimal drift in the total energy was observed until 0.82 ps into the simulation when the CO_2 molecule was observed to bind to an oxygen site. Analysis of the E(t) reveals a mean binding energy of ~ 2.82 eV (272 kJ/mol)for the CO_2. The resulting configuration is shown in Figure 8, and consists of a CO_3 type propeller structure characteristic of carbonate ($MgCO_3$). Several other runs, initiated under similar starting conditions, led to the same final structure, but involving other (similar) low-coordination oxygen sites.

Our simulation results strongly suggest that once access to low-coordination oxygen sites is available, the mechanism for precursor formation proceeds quite readily. Conversely, a stoichiometric lizardite structure may only allow CO_2 to permeate the gallery between layers (with ~ 2 Å clearance). The conformational restriction on CO_2 together with its interaction with essentially saturated oxide and hydroxyl sites, means that carbonate formation should be strongly precluded. It is in fact not observed, as confirmed by a recent synchrotron study which we undertook to establish that untreated lizardite feedstock does not readily carbonate, even when

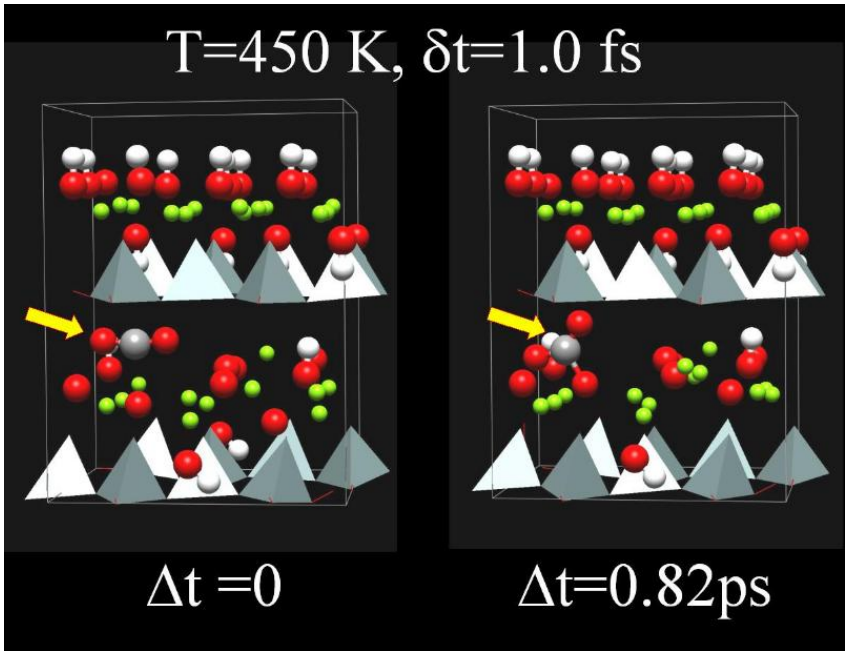

Figure 8: Quantum molecular dynamics simulation of a CO_2 molecule interacting with meta-lizardite. The yellow arrows indicate the position of the CO_2 molecule. Left frame: initial configuration, as described in the test. Right frame: Stable binding configuration of CO_2 in the bulk defective mineral. Note the minimal structural perturbation to the top lizardite-like layer. The carbonate precursor is seen as the propeller structure formed from the CO_2 and an under-coordinated oxygen atom in the right panel. (Legend: H=white, Mg=green, O=red, SiO_4=grey)

subjected to high temperatures and CO_2 pressures. Another intriguing formation mechanism could occur near the free surface of the meta-lizardite. Namely, the newly formed $MgCO_3$ precursor formed in the near-surface region of the mineral may subsequently diffuse out into the solution and provide a nucleation site for further carbonate growth in solution. Because of its potential importance to the overall reactions being studied, we plan on exploring this idea in more detail in

YEAR 2 studies which will focus on the mineral-solution interface and the aqueous carbonation of meta-lizardite.

3.1.2 SPECTROSCOPIC CHARACTERIZATION

3.1.2(a) Vibrational Spectra: Phonons

The Γ-point vibrational spectrum of lizardite was computed using a frozen phonon approach. An 18-atom unit cell of 1T-lizardite was first structurally optimized to obtain a minimum energy configuration. The DMol^3 code[17] with the Perdew-Wang local exchange-correlation functional[18], and an accurate double numerical basis set with polarization (DNP[19]) was used to compute the dynamical matrix using a five-point finite difference scheme 0.01Å atomic displacements. The mass-weighted Hessian was then diagonalized to yield 54 normal modes. The full spectrum will be discussed in detail in a subsequent publication. Here, for the purpose of elucidating the dehydroxylation behavior of lizardite in the context of heat-treatment, we focus on the hydroxyl bands.

The results are summarized in Figure 9 below, where it is seen that the manifold consists of two non-degenerate modes of frequency 3683 and 3642 cm^{-1}, and a pair of degenerate modes at 3614 cm^{-1}. In order to facilitate the discussion we have inset a structural model of the unit cell, with the silica "cage" hydroxyls denoted by the subscript "C", and the "brucite"-like hydroxyls indicated by a subscript "B". With respect to the space group symmetry of the unit cell, *P3m1*, the latter reside on (3c) sites having C_3 symmetry, while the "cage" hydroxyls occupy (1a) sites possessing C_{3v} symmetry. From factor group analysis it follows that the stretching hydroxyl modes are active in both the Raman and IR. The hydroxyl band portion of a Raman spectrum collected in our laboratory is shown in Figure 9(b) and confirms that the primary OH vibrational bands are common to both spectra. In our preliminary work we did not compute the intensities, but from the displacement patterns indicated by the eigenvectors in the figure we expect the two non-degenerate modes at 3642 and 3683 cm^{-1} to be dominant. In the literature on FTIR spectroscopy of serpentine minerals, reference is frequently made to bands associated with "inner" and "outer" hydroxyl motion. Our calculated eigenvectors indicate that the highest frequency band is due to the motion of the hydroxyls located within the silica cages, while the 3642 cm^{-1} band is associated with "brucite"-like hydroxyls denoted by "B" subscripts in the figure inset.

To address the possible effects due to impurities such as iron on the hydroxyl band frequencies, we repeated the calculations using the above procedure, but for the hypothetical phase $Mg_2FeSi_2O_5(OH)_4$. The resultant eigenvectors were found to be almost identical to those reported in Figure 5 while the OH bands are slightly shifted to lower frequencies (3668, 3626, 3601, 3601 cm^{-1}). Recent by studies by other groups[20] have also shown that a detailed analysis of the OH stretching bands between 3500-3700 cm^{-1} can be used to distinguish between different serpentine polymorphs even when other natural or synthetic minerals are present within the samples. The interlayer OH frequencies generally shift downwards in going from chrysotile to lizardite to antigorite. Such information can be used to accelerate the development of a practical carbonation reactivity matrix for serpentine feedstock materials by providing a efficient, low-cost screening/characterization technique for use in the field separation of serpentine feedstock materials.

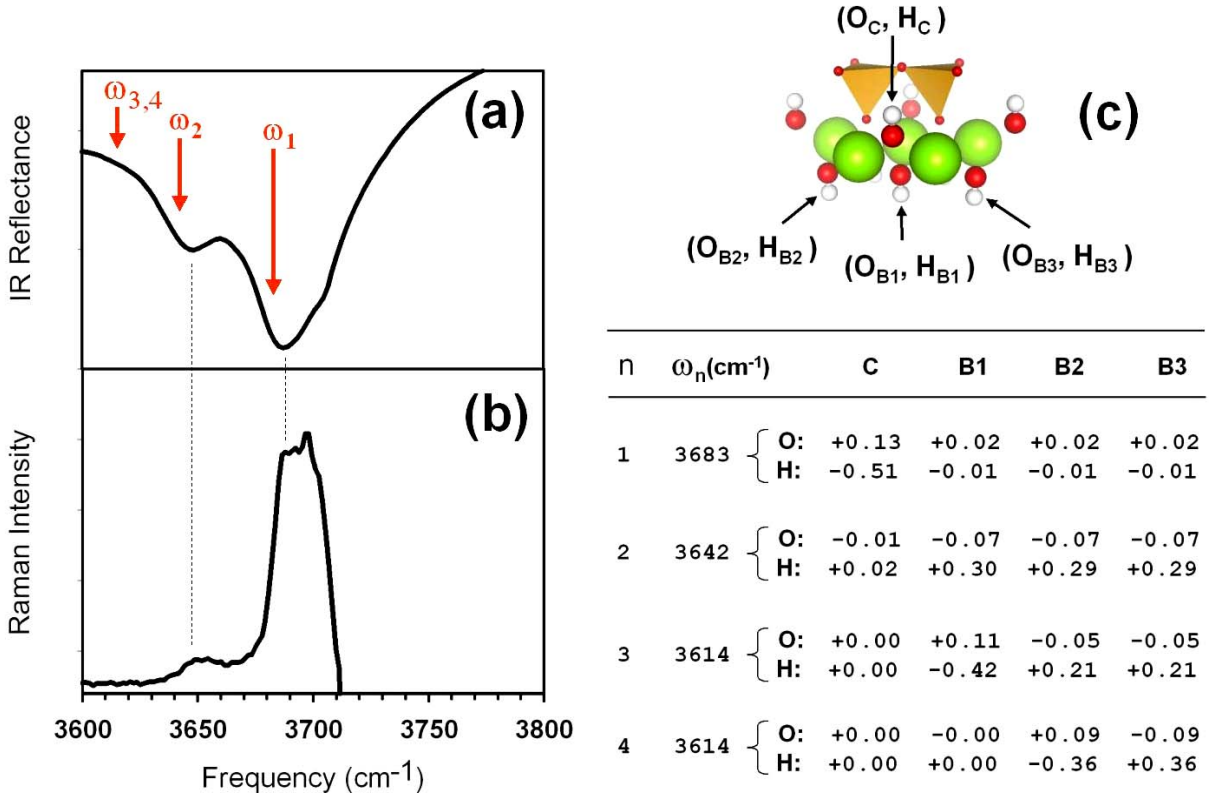

n	ω_n(cm^{-1})		C	B1	B2	B3
1	3683	O:	+0.13	+0.02	+0.02	+0.02
		H:	-0.51	-0.01	-0.01	-0.01
2	3642	O:	-0.01	-0.07	-0.07	-0.07
		H:	+0.02	+0.30	+0.29	+0.29
3	3614	O:	+0.00	+0.11	-0.05	-0.05
		H:	+0.00	-0.42	+0.21	+0.21
4	3614	O:	+0.00	-0.00	+0.09	-0.09
		H:	+0.00	+0.00	-0.36	+0.36

Figure 9: Summary of hydroxyl band vibrational analysis: (a) Observed OH-band infrared spectrum of Globe A Lizardite, (b) observed OH-band Raman spectrum of Globe A Lizardite, (c) Schematic of the unit cell of Lizardite indicating the species labeling. The accompanying table lists the computed frequencies and mass-weighted eigenvectors describing the atomic displacement patterns corresponding to each mode. (Legend: H=white, Mg=green, O=red, SiO_4=gray.)

3.1.5 Energy Loss Near Edge Spectra (ELNES) of Lizardite

Electron Energy Loss Spectra (EELS) and vibrational spectra (IR/Raman) can be used to help characterize, or "fingerprint", hitherto unknown intermediate materials formed during dehydroxylation/carbonation by providing an interpretation of the corresponding observed spectra in actual experiments. In principle, this provides an important bridge between the atomic level structure of the material and the energy loss spectrum at various energies. We have used state-of-the-art first principles simulations to generate very detailed information about the source of EELS spectral features. The near edge structure is approximately related to the conduction band density of states, and variations in magnitude as a function of energy loss are related to differences in the chemical environment for each constituent (*e.g.*, oxygen, carbon). We employed the full potential linearized augmented plane wave (FPLAPW) method as implemented in the WIEN2k program[21] to compute the Energy Loss Near Edge Spectra (ELNES) within the generalized gradient approximation (GGA). Full dynamic form factors were computed using crystalline Bloch states[22]. The latter were generated using the well-converged structures obtained earlier (as described in section 3.1 above). A broadening function of ~ 2eV was applied to the raw spectra to simulate experimental conditions.

The symmetry of the lizardite unit cell suggests oxygen K-edges should be a very sensitive probe of local bonding and structure. This is because oxygens are present in the tetrahedral framework, the magnesium layer and in the hydroxyl layer. This is less true for Magnesium and Silicon L_{23} edges, which are expected to be less rich in structure due to their simpler range of coordination within the crystalline environment. For the oxygen *K*-edge, differences in bonding character for chemically distinct oxygen sites within the crystal yield individual weighted contributions to the total cross-section, as shown in Figure 10, above. Thus, with reference to the total curve (black) and the violet curve, the shoulder feature at edge onset near 5 eV can be seen to be due to silica cage hydroxyl oxygen. The prominent feature at 15 eV is due to Mg near neighbor oxygens *e.g.*, apecal tetrahedral oxygens and "brucite-like" hydroxyl oxygens denoted by the red and blue curves, respectively. Apecal oxygens are also clearly responsible for the main feature near 22 eV (enhancement in energy loss coming from the red curve). Similarly, the 34 eV feature is mainly related to brucite hydroxyl oxygens.

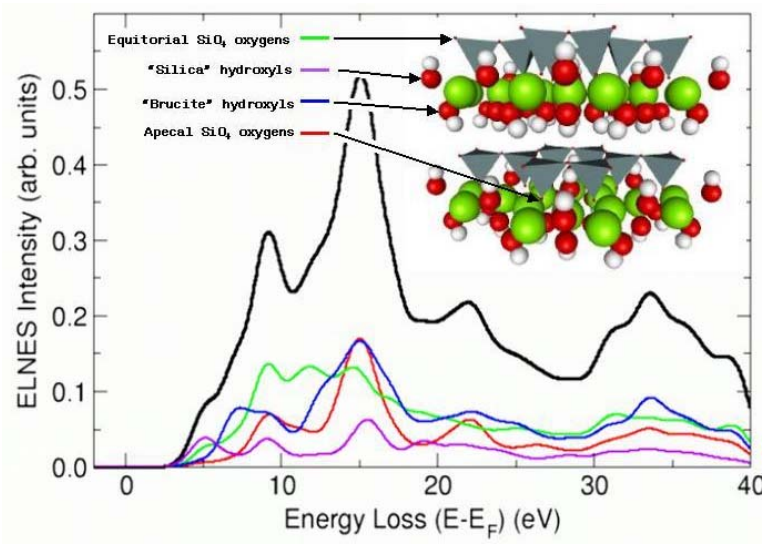

Figure 10: Composite figure containing a schematic representation of the 1T lizardite structure (inset) as well as the predicted oxygen K-edge electron energy loss structure (black curve). The individual colored curves represent the contributions to the full spectrum arising from difference oxygen sites within the crystal (see explanation in text).Legend: H=white, Mg=green, O=red, SiO_4=gray.

Experimental EELS analysis of the baseline lizardite as well as a series of meta-serpentines prior to and after carbonation, are planned in the coming year. Predictive calculations of the energy loss spectrum similar to those described here, will be used in conjunction with the baseline spectrum of the unaltered lizardite to interpret the structural changes induced by heating, leaching and carbonation.

3.2 SIMULATIONS OF THE CARBONATE PRODUCT

3.2.1 Origin of Low-angle MIES Scattering in Synchrotron Data

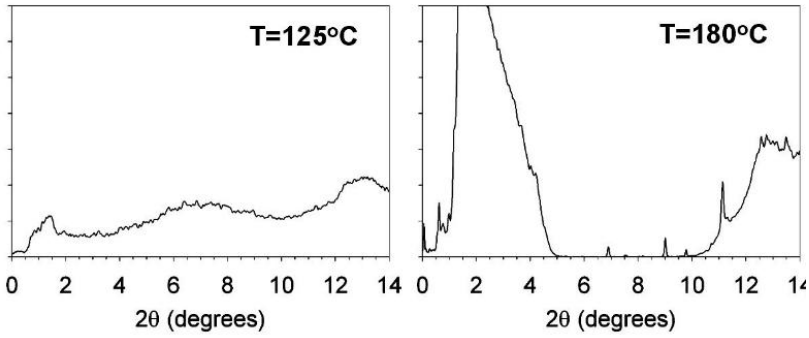

Figure 11: Integrated synchrotron diffraction data of the 640°C meta-serpentine sample in a $NaCl/Na_2CO_3$ solution after introduction of CO_2 at 1250 psi. Carbonate formation onset occurs upon heating to ~150°C. Left panel: "Amorphous" signature of the partially decomposed lizardite prior to carbonate formation. Right panel: Spectrum taken at 180°C showing carbonate peaks (2θ ~6-12 degrees) and large low-angle feature with an onset near 0.5 degrees.

Particle Scattering Effects in the small-angle XRD spectrum of 640oC heat-treated sample after carbonation: The objective of this study is to try to provide an explanation for the large intensity scattering signal found in the 640°C sample at reaction conditions (*e.g.*, upon carbonation). As shown in Figure 12 the relevant spectral feature spans the small-angle region in the vicinity of 2θ ~ 2°. We used the Cerius[2] simulation package to investigate the relationship between inter-particle distance, wavelength and particle size. In our straightforward approach we placed small (~ 1-10 *nm*) "carbonate" particles with definite internal crystalline structure on a large supercell (grid) of size D (~1-10 *nm*) as shown in Figure 12 below. Figure 13 shows the relationship between d, D. The incident radiation wavelength was taken to be 0.3311 Å as in the synchrotron experiments. Many of these simulations require several hours on a typical SGI workstation because effectively millions of reflections must be computed to produce a spectrum. Our largest carbonate "chunklette" (d~32 Å) contains about 1600 atoms.

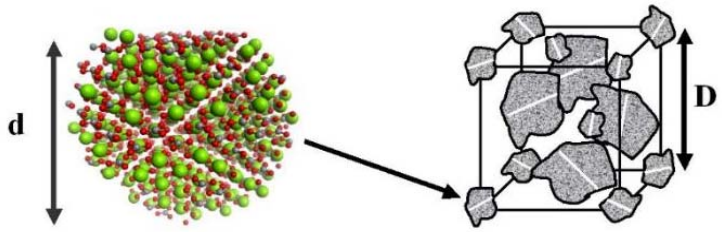

Figure 12: Figure illustrating the construction of a simple particle-scattering model. In this case carbonate "chunks" of diameter *d* are placed in a large cell of edge length D. In the example above D is approximately equal to the inter-particle distance.

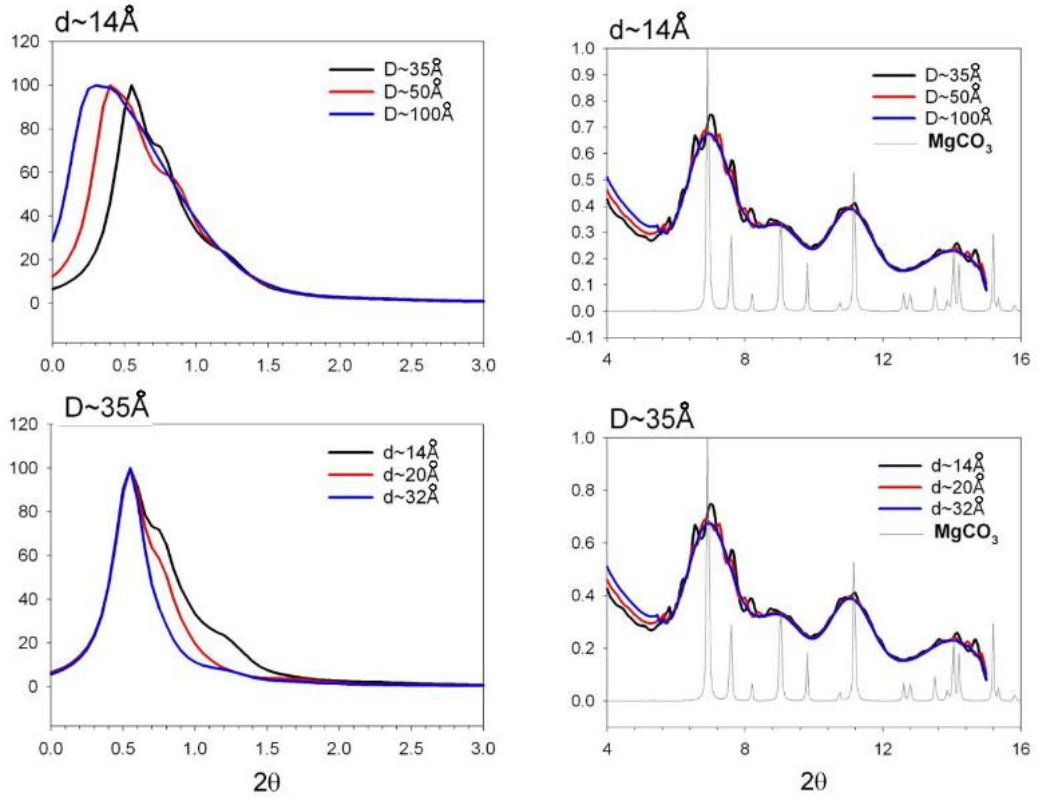

Figure 13: Representative simulation results of particle scattering effect. The top panels display the low-angle behavior while the bottom panels show the emergence of crystalline signatures at higher angles. In this example the broadened peaks reflect the position of carbonate features. The latter are shown (for a carbonate powder of particle size ~ 500 Å) as a gray XPD spectrum.

The simulated trends indicate that the onset of particle scattering for fixed particle size occurs at larger angles in proportion to the inter-particle distance (see d vs.D plots below). A surprising amount of structure is observed for fixed inter-particle distance as the particle size is varied. In particular, we find that for small d/D ratios, the low-angle spectrum is the most diffuse. Preliminary results for d/D in the large D limit show that onset of the particle scattering effects can be shifted to larger and larger 2θ values. Note that thesimulations were carried out for carbonate particles in an otherwise empty cell. It is likely that the residual silica matrix may provide the dominant particle scattering contribution, but we have shown that the main effect on the low-angle structure of the XPD is mostly independent of the precise nature of the particles. Further studies to validate this concept are currently underway under the pretext of spectroscopic modeling in support of experimental understanding, which extends into the YEAR 2 performance period.

4. CONCLUSIONS

Simulations are most useful when they are carefully designed to answer questions relevant to a specific experimental investigation or technical problem. Close integration of theoretical modeling/simulation with experiment has led to scientific insight that is difficult to achieve independently – a powerful synergy. These notions exemplify the strategy in the present Innovative Concepts Award and we shall continue to integrate advanced quantum mechanical modeling with Dynamic High Resolution Transmission Electron Microscopy (DHRTEM), Electron Energy Loss Spectroscopy (EELS) and infrared (IR) and Raman spectroscopy. The objective is to develop a detailed understanding of carbonation for the model Mg-rich lamellar hydroxide based minerals including lizardite, chrysotile and antigorite which ultimately will lead to the optimization of the relevant CO_2 mineral sequestration reaction processes, and a reduction in process cost. Such advances in fundamental understanding are absolutely essential to the accelerated development of viable CO_2 sequestration technology.

To our knowledge the work presented here represents the first *ab initio* investigation into the combined structural, electronic and vibrational properties of serpentine minerals. It is important to emphasize the role of *ab initio* modeling in the investigation of complex geochemical systems. Our calculations demonstrate that significant insight into the atom-level processes can be obtained from a predictive modeling approach.

5. REFERENCES

[1] H. Courtright, *Proceedings of the 17th International Pittsburgh Coal Conference,* Sec. 18-A, p. 8-20, Badie I. Morsi, *Ed.*, University of Pittsburgh Press, Pittsburgh; *ibid.* B.T. O'Neil., Sec 18-A.

[2] *Carbon Sequestration Research and Development*, Offices of Science and Fossil Energy, U.S. Department of Energy (December 1999).

[3] W. Seifritz, *Nature* **345**, 486 (1990).

[4] K. Lackner, D. Butt, C. Wendt, F. Goff, G. Guthrie, Los Alamos National Laboratory Technical Report LA-UR-97-2094 (1997).

[5] K.S. Lackner, C.H. Wendt, D.P. Butt, E.L. Joyce & D.H. Sharp, *Energy*, **20**, 1153 (1995). D.P. Butt, K.S. Lackner, C.H. Wendt, S.D. Conzone, H. Kung, Y.C. Lu & J.K. Bremser, *J. Am. Ceram. Soc.*, **79**, 1892 (1996). K.S. Lackner, D.P. Butt, C.H. Wendt, *Energy Convers. Mgmt*., **38**, S259 (1997).

[6] O'Connor, W.K.; Walters, R.P.; Dahlin, D.C.; Rush, G.E.; Nilsen, D.N.; Turner, P.C.; *Proc. 26th International Technical Conference on Coal Utilization & Fuel Systems*, pp. 765-76 (2001).

[7] M.J. McKelvy, R. Sharma, A.V.G. Chizmeshya, R.W. Carpenter & K. Streib (2001) *Chem. Mater*. **13**, 921-6 (2001); M.J. McKelvy, R. Sharma, A.V.G. Chizmeshya, H. Bearat, and R.W. Carpenter, *Proc. 25th Int. Tech. Conf. Coal Util. & Fuel Sys.*, 897 (2000).; H. Bearat, M.J. KcKelvy, A.V.G. Chizmeshya, R. Sharma & R.W. Carpenter, (2001) *J. Am. Ceram. Soc.* (in press.)

[8] W. K. O'Connor, D. C. Dahlin, D. N. Nilsen, R. P. Walters, and P. C. Turner, pp153-64 in *The Proceedings of the 25th International Technical Conference on Coal Utilization & Fuel Systems* (Clearwater, Florida, March 2000).

[9] G. Kresse and J. Furthmuller, *Comput. Mater. Sci.* **6**,15 (1996); G. Kresse and J. Hafner, *Phys. Rev. B* **4**7, 558 (1993); G. Kresse and J.J. Furthmuller *ibid.* **5**4,11 169 (1996).

[10] W. Kohn, *Reviews of Modern Physics*, Vol. 71, No. 2, Centenary (1999).

[11] D.M. Ceperley and B.J. Alder, *Phys. Rev. Lett.* **45**, 566 (1980).

[12] *"Mineral Physics and Crystallography: A Handbook of Physical Constants*", *Ed.* T.J. Ahrens, American Geophysical Union, Washington, DC, 1995.

[13] Guggenheim, S. and Zhan, W. *The Canadian Mineralogist* **36**, 1587 (1998).

[14] We computed a binding energy of –11.437 eV for H_2O(g) by placing the molecule into a cubic supercell with edge length 10 Å. The experimental sublimation energy of ice (~ -0.49 eV [Ref.15]) was then added to this number to obtain the binding energy of ice, -11.927 eV.

[15] James, A.M.; Lord, M.P. *Macmillan's Chemical & Physical Data*, (Macmillan Press LTD, London, 1992).

[16] D. Ochs, M. Brause, B. Braun, W. Maus-Friedrichs, and Kempter, *Surf. Sci.* **397**, 101 (1998).

[17] Delley, B. J. Chem. Phys. **113,** 7756 (2000).

[18] J. P. Perdew and Y. Wang, Phys. Rev. B **45**, 13244 (1992).

[19] Delley, B. J. Chem. Phys. **92,** 508 (1990).

[20] Lemaire, C.; Guyot, F.; Reynard, B. (private communication), also see http://www.campublic.co.uk/science/publications/JConfAbs/4/652.html

[21] P. Blaha, K. Schwarz, and J. Luitz, WIEN97, A Full Potential Linearized Augmented PlaneWave Package for Calculating Crystal Properties (Karheinz Scharwz, Techn. Universitat Wien, Austria), 1999. ISBN 3-9501031-0-4. Blaha P, Schwartz K, Dufek P and Augustyn R 1995 *WIEN95* Technical University of Vienna. Improved and updated Unix version of the original copyrighted WIEN code, P.Blaha, K Schwartz, P Sorantin and S B, Trickey *Comput. Phys. Commun.* **59** 399 **(**1990).

[22] Nelhiebel, M., Louf, P.-H., Schattschneider, P., Blaha, P., Schwarz, K. and Jouffrey, B. Theory of orientation-sensitive near-edge fine-structure core-level spectroscopy. *Phys.Rev.B* **59**, 12807 (1999).

6. APPENDIX 1 : ARTICLES, PRESENTATIONS, AND STUDENT SUPPORT

(i) Publications (in preparation)

"*Ab Initio* investigations of Dehydroxylation Reactions in 1T-Lizardite", Andrew V.G. Chizmeshya, Deirdre Gormley, Otto F. Sankey and Michael J. McKelvy, *to be submitted.*

"Infrared and Raman Spectroscopic Interpretation of the Dehydroxylation of Lizardite: An Experimental and Theoretical Study", Jason R. Diefenbacher, Andrew V.G. Chizmeshya, George H. Wolf and Michael J. McKelvy *to be submitted.*

(ii) Publications (in print)

"Developing a Mechanistic Understanding of Serpentine CO2 Mineral Carbonation Reaction Processes", Michael J. McKelvy, R. Sharma, R.W. Carpenter, George Wolf, Andrew V.G. Chizmeshya, Hamdallah Bearat and Jason Diefenbacher, *Proc. 27th Int. Tech. Conf. On Coal Util. And Fuel Syst*, Vol.1, 791-802 (2002).

"Atomic-level Understanding of CO2 Mineral Carbonation Mechanisms from Advanced Computational Modeling", Andrew V.G. Chizmeshya, Otto F. Sankey, Michael J. McKelvy, R. Sharma, R.W. Carpenter, George Wolf, Hamdallah Bearat and Jason Diefenbacher, *Proc. 27th Int. Tech. Conf. On Coal Util. And Fuel Syst*, Vol.1, 803-814 (2002).

(iii) Conference Presentations

"CO_2 Mineral Sequestration: An Opportunity for Materials Science in Greenhouse Gas Mitigation Technology", A.V.G. Chizmeshya, Department of Physics and Astronomy, November 7, Tempe, Arizona (2002).

"Fundamental modeling of pre-carbonation treatment effects on serpentine and olivine feedstock", A.V.G. Chizmeshya, National Mineral Carbonation Working Group Meeting, Sept 9-10, U.S. Department of Energy, Office of Fossil Energy, Albany Research Center, Albany, Oregon (2002).

"Application of First principles Simulation to CO_2 Mineral Sequestration", A.V.G. Chizmeshya, 17th International Coal Conference, March 11-14, Clearwater, Florida (2002).

(iv) Students Supported under this Grant

Michael Kocher: Undergraduate research assistant, jointly enrolled in the Physics and Chemistry programs at Arizona State University.

Deirdre Gormley: Doctoral candidate in the Science and Engineering Materials Ph.D. Program at Arizona State University.

APPENDIX 2 : WORK PLAN

Work Plan Guide reproduced from the original Proposal:

"The timeline for the proposed work will closely parallel that of the joint ASU/ANL study in order to maximize the impact of the modeling/simulation results, and support the overarching need to efficiently explore ways to optimize serpentine carbonation. Key activities are summarized in the table below. The major focus areas, (i) surface reconstruction/heat-activation

ACTIVITY	YEAR 1	YEAR 2	YEAR 3
Computer Hardware and Software Installation, Configuration and Benchmarking			
Heat-activation (dehydroxylation) Studies of surface reconstruction			
Fluid phase carbonation mechanisms & reaction rate modeling			
EELS, XRD and Vibrational Spectroscopic Simulation			
Modeling defects/impurities and their effect on reactivity			
Technical Progress Reports			
Contractors Annual Review Meeting			
Final Year Peer Review Meeting			

effects, (ii) fluid-phase carbonation mechanism modeling, and (iii) modeling of impurity/defect effects on carbonation, are timed to optimize the overlap with anticipated within the parallel experimental study. The calculation of electron energy-loss spectra, vibrational (IR and Raman) and XRD patterns derived from structural modeling will be ongoing throughout the performance period of the project. Specific studies will complement, and be guided by, the ASU-ANL serpentine carbonation experiments."